How cohesion controls the roughness of a granular deposit

Anaïs Abramian, Pierre-Yves Lagrée, Lydie Staron

Soft Matter

ARTICLE TYPE

Cite this: DOI: 00.0000/xxxxxxxxxx

How cohesion controls the roughness of a granular deposit†

Anaïs Abramian,*[a] Pierre-Yves Lagrée,[a] and Lydie Staron[a]

Received Date
Accepted Date

DOI: 00.0000/xxxxxxxxxx

Cohesive granular materials often form clusters of grains, which alter their flowing properties. However, how these clusters form and evolve is difficult to visualize in the bulk of the material, and thus to model. Here, we use a proxy to investigate the formation of such clusters, which is the rough surface of a cohesive granular deposit. We characterize this roughness and show how it is related to the cohesion between beads. Specifically, the size of this roughness increases with the inter-particle cohesion, and the profile exhibits a self-affine behaviour, as observed for crack paths in the domain of fractography. In addition to provide a simple method to measure the inter-particle cohesion from macroscopic parameters, these results give a better comprehension of the formation of clusters in cohesive granular materials.

1 Introduction

Cohesion forces between grains strongly alter the flow of a granular material. Instead of flowing homogeneously, grains often aggregate and form clusters in the bulk of the material. In an industrial context, this aggregation is sometimes desired for mixing or granulation processes[1], but can also slow down the flow of a production chain, and even clog a conveyor or a silo[2]. Overall, a better handling of these materials requires to characterize properly their flowing properties. More generally, these cohesive flows are encountered in many other situations, such as soil stability or debris flows. However, what controls the size and the dynamics of the aggregates, from a fundamental point of view, remains an active matter of research.

Most studies on the dynamics of aggregation focused on wet granular materials, for which cohesion is induced by capillary bridges between grains through a small amount of liquid. In this context, different configurations have been investigated, such as the formation of aggregates in rotating drums[3], in a vibrated shaker[4], or at the surface of stationary flows[5]. All these studies show that the cluster size increases with liquid contents, and, to a lesser extent, with the flow dynamics or the grain inertia. To explain this behaviour, it is possible to visualize the liquid bridges distribution, forming the clusters in the bulk of material, using fluorescence confocal microscopy[4] or X-ray microtomography[6]. The peculiar distribution of liquid then enables to relate the mechanical properties of the material. This visualization however requires heavy techniques and is only possible for a static material.

[a] Sorbonne Université, CNRS, Institut Jean Le Rond d'Alembert, F-75005 Paris, France; E-mail: anaisabramian@gmail.com

An easier, although indirect, visualization of this distribution is possible through the shape of a fracture formed in the material. Indeed, Tapia *et al.*[7] recently characterized the profile of a fracture produced in a thin layer of a humid granular material, by controlling the humidity of the surrounding atmosphere. Using a statistical approach, they showed that the typical size of the roughness is related to the cluster size, L, which is strongly correlated to the liquid content, and therefore to the number of cohesive bonds. However, cohesion force between grains is then a complex function of the bond's shape. It is thus difficult to relate the cluster size to the grain-scale cohesion forces.

An alternative to the liquid-induced cohesion was recently proposed by Gans *et al.*[8], who synthesized a cohesion-controlled granular material. This sticky material is made of polymeric coated beads, which enables to tune easily the cohesion of the bulk by varying the concentration of the polymeric solution. This allowed them to relate the macroscopic properties of the material to the grain-scale forces, which facilitates models in the perspective to investigate the rheology of such a material.

Another option to investigate the influence of cohesion in the flow of a granular material is to adopt a numerical description of cohesive forces at the grain scale using discrete methods. In this case, adhesive forces result from a cohesive contact model, either explicit in Discrete Elements Methods[9–11], or implicit in Contact Dynamics algorithms[12,13]. Despite the use of simple interaction models, the presence of cohesion reveals a rich dependency of the flow with numerical parameters, contrary to dry granular materials. In discrete element methods, the flow becomes sensitive to the stiffness and the elasticity modulus of the grains[14]. In contact dynamics, where particles are perfectly rigid, this dependency translates into a contribution of the time step into the dynamics equations[15]. Overall, the introduction of a single dimensionless

Label	Initial height	Initial config.	Number of grains	Bond numbers
1	$45d$	11	5572	0, 10, 20, 30, 40, 50
2	$67.5d$	5	8358	10, 30, 50
3	$90d$	5	11144	10, 30, 50
4	$264d$	3	33432	10, 30, 50

Table 1 Table of parameters for numerical simulations.

number accounts for this dependency. In the present paper, we will use a code based on contact dynamics, where simulations are performed with a fixed time step corresponding to a weaker influence of the latter and small averaged error[16].

Based on this numerical scheme, we investigate here the formation of clusters in cohesive granular materials in a simple configuration: the collapse of a granular column. When a column of cohesionless grains is released under its own weight, it flows until the deposit reaches the angle of repose, $\arctan(\mu_s)$, where μ_s is the static friction coefficient. The surface of the final deposit is then perfectly smooth, exhibiting only a grain-size roughness. However, when cohesion is introduced, the final deposit features a different, larger roughness. Here, we characterize the statistical properties of this roughness, and show that the morphology of the final deposit is an immediate signature of cohesion and cluster size. This correlation provides a direct measurement of the inter-particle cohesion forces, in addition to other characterizations of the mechanical properties of a cohesive granular material or a powder[17].

The present article is organized as follow. We first describe the numerical simulations, and then analyze the statistical parameters of the roughness. Finally, we relate these parameters to the inter-particle forces, and compare this study to recent experiments of cohesive granular collapses.

2 Numerical simulations

We perform a series of numerical simulations based on a Contact Dynamics algorithm in two dimensions[18–20]. This algorithm follows the equations of the dynamics for each perfectly-rigid grain while obeying the contact laws, through an implicit method.

The grains interact at contact through Coulombic friction, involving the grain-scale friction coefficient μ, set to 0.2 and not varied in this study. The contacts are made cohesive through the introduction of a cohesive threshold F_c in the unilaterally Sigorini's graph. We associate, to this cohesion force, the dimensionless Bond number[11,21]:

$$\mathrm{Bo} = \frac{F_c}{mg}, \tag{1}$$

where m is the mass of a grain, and g is gravity. The Bond number provides a definition of cohesion at the grain scale, and is thus pertinent for discrete numerical simulations. However, at the material scale, we can define a cohesive length ℓ_c, defined as:

$$\ell_c = \frac{\tau_c}{\rho g} \tag{2}$$

where τ_c is the yield stress of the material and ρ its density. This

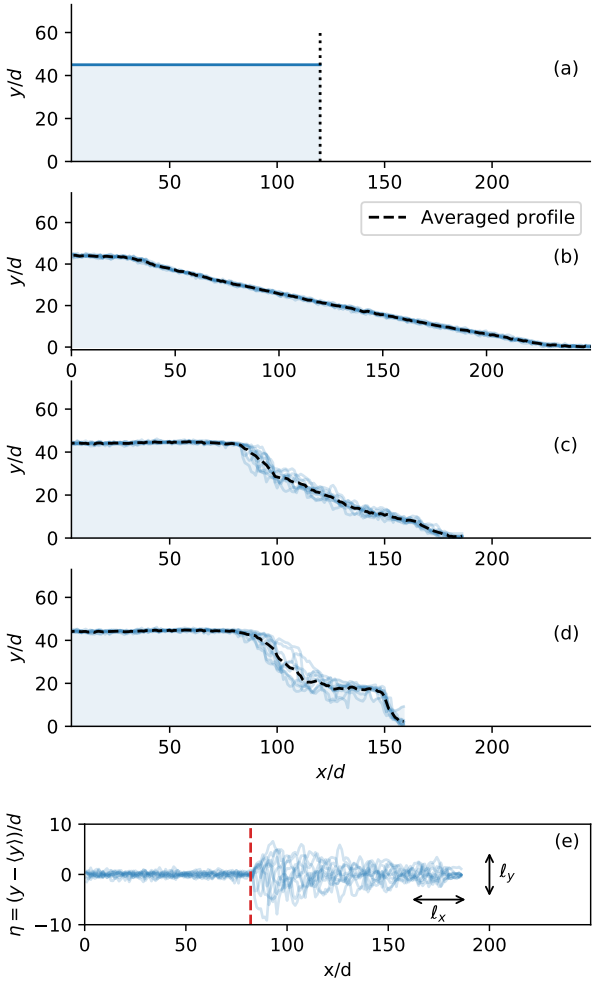

Fig. 1 Fluctuation of the final deposits around their mean profile. Blues lines : 10 simulations made in the same configuration, but varying the initial state. Dashed black line : average profile over the 10 simulations. (a) Initial column. (b) Final deposit. $\mathrm{Bo} = 0$. (c) Final deposit. $\mathrm{Bo} = 20$. (d) Final deposit. $\mathrm{Bo} = 50$. (d) Deposit profiles subtracted by their average over 10 collapses for $\mathrm{Bo} = 20$. Dashed red line: limit between static grains and flowing grains. The longitudinal length ℓ_y and the transverse length ℓ_x are sketched.

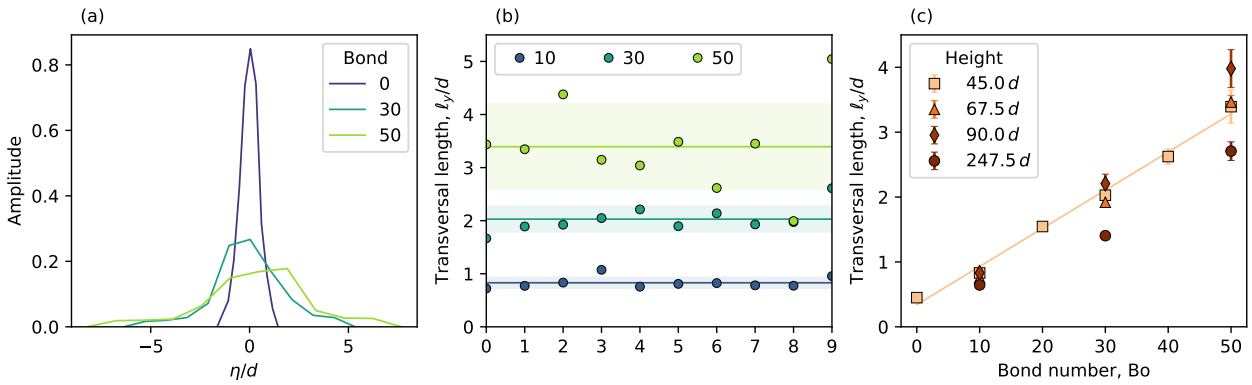

Fig. 2 Amplitude of the fluctuations. (a) Probability density function of η for the simulations of initial column H$= 45d$, and for different Bond numbers. (b) Standard deviation of the fluctuations for each simulation of initial column H$= 45d$, and for different Bond numbers. We define ℓ_y as the average of this standard deviation over the simulations. The colored area corresponds to the standard deviation of this length over the 10 simulations. (c) Typical height of the fluctuations ℓ_y as a function of the Bond number for different initial geometries of the column. Errorbars are the standard deviation of ℓ_y over N simulations divided by $\sqrt{N}$.

is a definition of cohesion at the material scale. To bridge the gap between these two scales, we can use the approach of a previous study[13], by measuring the threshold of stability of a cohesive granular column, and comparing it to its theoretical value, which depends on the yield stress of the material described by a cohesive rheology. This provides a relation between the Bond number and the cohesive length, $\ell_c \sim 0.8\,\mathrm{Bo}/d$, which will be useful in the following.

At the beginning of a simulation, we first build a column by simulating a random rain of $N_g = 5572$ grains in the gravity field. The diameter of the grains is randomly distributed between 4 mm and 6 mm, so that the particle mean diameter is $d = 5$ mm. In a first series of numerical simulations, the initial height of the column is fixed at $H = 22.6\,\mathrm{cm} = 45d$, and its radius at $R = 60\,\mathrm{cm} = 120d$, leading to an aspect ratio of $a = H/R = 0.4$ [Fig. 1(a)]. This keeps us in a regime where the left wall is far enough from the right corner not to have any influence on the final deposit. After the initial configuration is built, the column is released and flows under its own weight, until it reaches a final runout. The bottom is made rough, as if grains were virtually glued on it, to ensure the no-slip condition during the collapse.

At the end of the collapse, the final shape of the deposit is then interpolated from the grain positions following the contour of the deposit with a binning window. We ensure that the size of this window is much smaller than the grain size, and we keep it constant for all the simulations.

For this given geometry, and at a fixed Bond number, we then reproduce 11 independent simulations varying the initial configuration, through randomly varying the distribution of grain diameters. A typical profile is plotted on Fig. 1(c) in blue, for a Bond number of Bo $= 20$. We then define the mean profile $\langle y \rangle$ of the collapse averaged over the 11 simulations [dashed black line in Fig. 1(b), (c), (d)].

We vary the Bond number from 0 to 50 and follow the same procedure. This gives us a total of 55 numerical simulations for one geometry of column. We did three additional series for different heights; the discussion on its influence is presented in section 4.2. The computation time varies from few hours to few days depending on the number of grains.

We can now observe the final shape of the deposit as a function of the Bond number, for a fixed initial height (Fig. 1). Without any cohesion (Bo $= 0$, the fluctuations around the mean profile virtually vanish, and all the profiles therefore match with the average. The fluctuations then increase with the Bond number, which suggests a strong correlation between the roughness of the deposit and the cohesion. In the next section, we describe quantitatively this observation.

Note that if the column is too small, the cohesion forces overcome the weight of the column; the column is thus stable and does not flow. Therefore, this threshold limits the range of Bond numbers and of initial heights for the column. This range is chosen to obtain unstable columns, or flowing columns, for which the weight overcomes the cohesion forces. This limit has been specifically investigated with this code and compared to a continuous approach, for which an analytical model is feasible[13]. For information, the threshold height column is about $20d$ for a Bond number of 50.

3 Roughness characterization

To measure quantitatively the influence of cohesion on the roughness of the deposit, we define the function η as the subtraction of the mean profile to the final deposit [Fig. 1(e)]:

$$\eta(x) = y - \langle y \rangle\,, \tag{3}$$

where $\langle \cdot \rangle$ denotes the average operator over the simulations of same parameters (ensemble mean). In the part laying on the left wall, the grains do not flow, and this function almost vanishes [before the dashed line, Fig. 1(d)]. When the grains flow, this profile features strong fluctuations around zero [after the dashed line, Fig. 1(d)]. The fluctuation height decreases with the x-coordinate. This is probably correlated with grain inertia, and thus with the distance travelled by grains during the collapse. Inertia induces fragmentation, and thus diminishes the fluctuations. However, as a first step towards the characterization of these fluc-

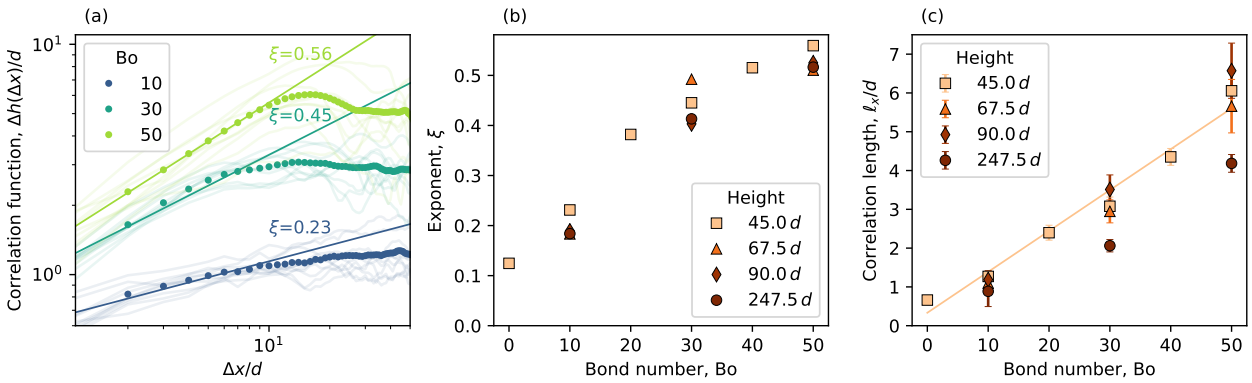

Fig. 3 Correlations of the fluctuations profile η. (a) Auto-correlation function of the fluctuations averaged over the N simulations, for different Bond numbers. We define ℓ_x as the maximum of this function. (b) Auto-correlation exponent of the fluctuations. Each color corresponds to a different initial height for the column. (c) Auto-correlation length of the fluctuations, ℓ_x, as a function of the Bond number. Errorbars are measured by taking the standard deviation of this length over the N simulations, divided by $\sqrt{N}$.

tuations, we do not study this influence. In the following, instead, we focus on the typical length of the fluctuations in the transverse direction, ℓ_y, and on their typical wavelength in the longitudinal direction, ℓ_x, as defined on Fig. 1(e).

Note that we subtract the average profile by following its vertical projection, instead of using the normal direction of the mean deposit. This may introduce a bias with the Bond number. However, as the slope of the deposit is not clearly defined, it is difficult to apply a reproducible procedure. Moreover, the probability distribution of η, plotted on Fig. 2(a), is symmetrical enough to allow us to neglect this effect. This distribution is peaked around zero for a cohesionless granular material, and then widens with the Bond number. Overall, these distributions are nearly gaussian, that allows us to define usual statistical properties for the profile η.

3.1 Standard deviation

We first define a characteristic length through the standard deviation of this distribution:

$$\ell_y = \sqrt{\langle \eta^2 \rangle_x - \langle \eta \rangle_x^2}, \tag{4}$$

where $\langle \cdot \rangle_x$ denotes the average over the coordinate x, this time. This length is found to be approximately constant from one simulation to another, although it varies in a tiny range around the average, corresponding to the errorbar [Fig. 2(b)]. We thus define the typical size of the fluctuations as the mean value of the standard deviations over the 11 simulations. We observe a strong correlation between this typical length and the Bond number, namely the cohesion between grains [Fig. 2(c)]. For cohesionless particles, the height of the fluctuations is typically a fraction of the grain size ($0.3\,d$), meaning that the roughness is only induced by the grains. It is then multiplied by a factor of 4 when the Bond number increases from 10 to 50. Thus, this length seems to be a reliable proxy for the cohesion of the material.

More precisely, we can try to compare this length to the natural length of the system: the cohesive length, ℓ_c, as mentioned in section 2 through equation (2). To do so, we use the relation between the Bond number and the cohesive length established in Abramian *et al.* [13], by comparing the stability threshold of a numerical discrete cohesive column. Following this relation, we obtain that the length ℓ_y increases proportionally with the cohesive length as:

$$\frac{\ell_y}{d} = 0.34 + 0.70\,\frac{\ell_c}{d}, \tag{5}$$

for a column of initial height equal to $H = 45\,d$ [Orange line, Fig. 2(c)]. This correlation qualitatively agrees with the experiments of Tapia *et al.* [7] on the roughness of a cohesive fracture, for which the size of the crack path fluctuations increase with relative humidity, and therefore with cohesion. At this step, however, we must be careful with the quantitative interpretation of the coefficients. The latter could depend on the nature of the grains, or on few numerical aspects; we discuss this point later in the article. We turn now to the characterization of the fluctuations through correlations, that could be more robust against numerical or experimental parameters.

3.2 Correlations

We characterize the correlations of the fluctuations through the height-height correlation function:

$$\Delta h(\Delta x) = \sqrt{\langle [\eta(x+\Delta x) - \eta(x)]^2 \rangle_x}, \tag{6}$$

where Δh is the height difference between two points spaced from a distance Δx.

This definition is commonly used in the community of fractography, to characterize a fracture surface or a crack path in materials [22]. In this context, the statistical properties of this correlation function reveal how cracks interact with the material microstructure and provide a description of the crack dynamics [22]. This subtracting correlation function can be generalized for two-dimensional roughness profiles, which provides the direction of propagation of the crack in the material. Following this approach, we analyze the correlations of the roughness profiles.

For these granular-deposit profiles, Δh starts from zero, increases with Δx until it reaches a plateau region [Fig. 3(a)]. For

Δx smaller than typically $10d$, this trend is reminiscent of a self-affine or a self-similar profile, for which:

$$\Delta h(\Delta x) \propto \Delta x^{\xi}\,, \tag{7}$$

where ξ is the roughness exponent, sometimes called the Hurst exponent in the fractography community[23]. The fluctuations of a crack path in a thin sheet also features a self-affine profile. Specifically, crack path profiles in different types of paper sheet display a roughness exponent of about $\xi \sim 0.7$ that varies weakly from one type of paper to another[22]. This exponent differs significantly for polystyrene panels or sandstone, with $\xi \sim 0.5$. These differences indicate two different failure behaviour : cracks in polystyrene follow a directed random walk, characteristic of a brittle crack growth ($\xi \sim 0.5$), whereas cracks in a paper sheet correspond to a propagation of the failure by damage coalescence and nucleation ($\xi > 0.5$)[24–26].

The self-affine behaviour has also been observed for fracture profiles in a humid granular material by Tapia *et al.*[7]. In this case, they showed that the exponent of the power law fit varies with the liquid content in the bulk of the material. However, as the grain-scale cohesion force is then a non monotonic function of the liquid content, the relationship between the exponent and cohesion is complex.

Our numerical simulations straightly yields the dependency of this exponent with the grain-scale cohesion forces: the roughness exponent increases with the Bond number through the curve plotted in Fig. 3(b). It starts from about 0.1 for a cohesionless material— a value significantly smaller than encountered for crack paths. It then reaches about 0.6 when increasing the Bond number towards 50, although following a nonlinear trend, resembling to a saturation for high Bond numbers. If this exponent depends only on the failure mechanism at the grain scale, as it is the case in the crack paths of heterogeneous materials, it could be a better proxy for cohesion than the length ℓ_y, but this question would require a dedicated investigation.

For Δx typically larger than about $10d$, the power-law fit then features a plateau [Fig. 3(a)]. We define ℓ_x as the maximum of this function $\ell_x = \max[\Delta h(\Delta x)]$, and find that this parameter, seen as a correlation length, also increases with cohesion. Precisely, by relating the Bond number with the cohesive length ℓ_c, ℓ_x follows the relation:

$$\frac{\ell_x}{d} = 0.55 + 1.2\,\frac{\ell_c}{d} \tag{8}$$

Here again, this length is controlled by the grain size for cohesionless material, and then increases linearly with the cohesive length. Here again, the quantitative interpretation of these coefficients may be affected by any other parameters, and must be taken with caution.

Finally, in the fracture surface context, experiments reveal the pertinence of the cutoff length, or crossover length scale, i.e. the abscissa of the intersection between the power law and the plateau variation of the correlation function[27]. In our system, these lengths could also capture the cohesive properties of the material. However, they are not well defined in our measurements, and seem to remain constant for almost all simulations, of the order of 10 grain diameters.

4 Discussion

4.1 Exploitation of the results

The numerical simulations presented here yield a clear relationship between roughness and cohesion: The two characteristic lengths, ℓ_x and ℓ_y, linearly increase with the cohesive length. If these relationships hold for any material, we could extrapolate the inter-particle cohesion only from the macroscopic properties of its roughness deposit. However, the coefficients involved in equations (5) and (8) have no reason to be universal, and should probably be calibrated according to the material. First, these coefficients could depend on the nature of the granular material, such as the grain size, or the friction coefficient.Secondly, they might be affected by numerical aspects, such as the interrelation between time-step and cohesion in contact-dynamics algorithms[16], or the dimension of the experiments.

As in the context of fractography, the roughness exponent ξ is potentially a more comprehensive proxy for cohesion, that could reveal the grain-scale origin of the roughness. If confirmed, its curve could allow for a direct measurement of cohesion without any calibration.

By plotting now the size of the vertical fluctuations of the surface ℓ_y as a function of the correlation length ℓ_x, we find them proportional (Fig. 4). This is consistent with the formation of clusters of size L on the surface of the material, which was investigated by Tapia *et al.*[7] in the case of a fracturing wet granular layer. We find that the longitudinal characteristic length ℓ_x is twice larger than the transverse one, ℓ_y. This factor 2 could come from the different definitions, and roughly coincides with the fact that the column spreads sideways to form a deposit with a small angle of repose of $\arctan(\ell_y/\ell_x)$, at least for small Bond numbers. More importantly, this linear relation states that only one characteristic size exists in this profile, probably that of the cohesive clusters.

By considering a unique characteristic length L, that we take arbitrarily equal to ℓ_x, we can compare it to a prediction made by Alarcon *et al.*[28], according to which:

$$\frac{L}{d} = \frac{1}{2} + \frac{\rho g d^3}{8\mu_s \beta}\,\frac{\ell_c}{d}\,, \tag{9}$$

where β is a coefficient taking into account the influence of the grain surface asperity or the liquid bond shape. This relation is not directly comparable with our data, as it holds for humid granular materials, but it is $0.5d$ for cohesionless particles, and then linearly increases with the cohesion length ℓ_c, as ℓ_x does in equation (8). It provides a rough order of magnitude for the cluster size in cohesive granular matter, that is between one and ten grain diameter.

4.2 Influence of the column's initial height

We characterized the roughness deposit of a given initial geometry, and showed that the size of the fluctuations increases with the inter particle cohesion. We now want to investigate the influence of the column's initial height, which should translate into a

change of flow inertia, as higher columns lead to larger and faster collapses. We expect more fragmentation as the flow is faster, and a size of aggregates which might therefore diminish.

To test this scenario, we now vary the initial height of the column. Over this range of Bond numbers, we cannot decrease the height because the column would not flow. We must therefore increase the height of the column, to remain in the unstable domain. However, increasing the height of the column means to increase the total number of grains, and thus the computation time. Therefore, we perform two series of 5 simulations, increasing the height by a factor 1.5 and then 2, and finally 3 additional simulations increasing the height by 5.5 (Tab. 1).

We apply the same procedure to measure the typical longitudinal length [Fig. 2(c)] and the typical transverse length [Fig. 2(b)]. Surprisingly, we do not observe a strong influence of the collapse dynamics. In particular, at a fixed Bond number, the length ℓ_y varies of about 10 % when the height is multiplied by a factor 2. Moreover, this variation is counter-intuitive as the fluctuations increase for higher columns, instead of vanishing, but this variation remains in the measurement uncertainties.

For a height factor of 5.5, we observe, this time, a significant change for ℓ_x and ℓ_y. The fluctuation size still increases with the Bond number, but all the lengths are smaller than in the previous configurations, as expected. This allows us to highlight a domain where inertia starts to play a significant role on the roughness deposit, but the effect of inertia would require a dedicated investigation.

4.3 Comparison with granular-collapse experiments

Granular collapse experiments are not rare in the literature. Since the pioneer studies on dry granular collapses [29–31], recent articles deal with humid granular collapse, from wet to fully saturated situations [32–35]. These articles focused on the runout distance; the shape roughness of the deposit is only barely mentioned. This is therefore difficult to compare this work with the present analysis, but we report here some interesting information in the light of our results.

Langlois *et al.* [33] investigated numerically the collapse of brittle material, where, contrary to our cohesive grains, bonds between grains are irreversibly broken during the collapse. As expected, the surface of the deposit is still qualitatively rougher as the Bond number increases. By attributing a color to each particle according to their vertical position, they show that (i) the statigraphy is not preserved, and that (ii) the deposit features blocks, sometimes of size comparable to the columns's height, laying on fine-grains material; superficial blocks are indeed subject to less stress and therefore remain roughly intact. This suggests a link between the surface roughness and the dynamics in the bulk of the material, which could be investigated further.

In a different way, Bougouin *et al.* [35] performed granular-collapse experiments of a fully saturated material, changing the initial column's height and the bead size. When the column flows, the deposit features either a block-avalanche profile or a continuous avalanche one, depending on the contribution of the capillary effects; this might introduce a nonlinear variation of the lengths ℓ_y and ℓ_x with the capillary length. Finally, experiments in the pendular regime [32,34] reveal the influence of the grain shape and grain size distribution on the flow. Although pictures also suggest a rough surface of the final deposit, these experiments reveal the existence of two distinctive angles, top and toe angles, in the final shape of the deposit. Note that in most experiments with humid granular materials, liquid bonds migrate, and lubrication effects can occur, which is not the case in our simulations.

Overall, only one series of cohesive granular collapse, made with the cohesion-controlled granular material described in the introduction [8], is directly comparable to our numerical simulations. This experiment, performed by Gans [36], was initially done to investigate the influence of cohesion on the runout length of the deposit. The material used is coated beads whom the cohesion is controlled and reproducible through the concentration of boric acid during the preparation. In this case, the concentration leads to a thickness of coating of 2.8 mm, resulting in a Bond number of about 8. The beads have a diameter of $d = 800 \pm 60\,\mu$m, and a friction coefficient of $\mu_s = 0.4$.

The material is initially set in a column of radius 6.6 cm, and of height 12 cm, providing an aspect ratio of 2. After the gate is removed, the column then flows under its weight, just as in our simulations. Repeating this experiment five times provide 5 experimental profiles for the final deposit. From these five profiles, we then measure the averaged profile that we subtract to all final deposits. We can thus apply the same procedure to measure ℓ_x and ℓ_y.

We find a transverse length of $\ell_y = (1.4 \pm 0.1)\,d$, which is significantly higher than the trend we found in our simulations. We did not report this point on the plot as there is several reasons why we cannot compare it. First, the grain size is much smaller compared to the height of the column, and the friction coefficient is also different. Second, the procedure to measure the Bond number relies on an experimental calibration which induces uncertainties. Finally, by looking at the correlations, we also find a self-afine profile, while the exponent is about 0.5. The correlation length is equal to $\ell_x = (2.3 \pm 0.2)\,d$.

This experimental data overall accords with the order of magnitude of our numerical simulations. Again, as the aspect ratio and the grain sizes are different, however, we can only be qualitative.

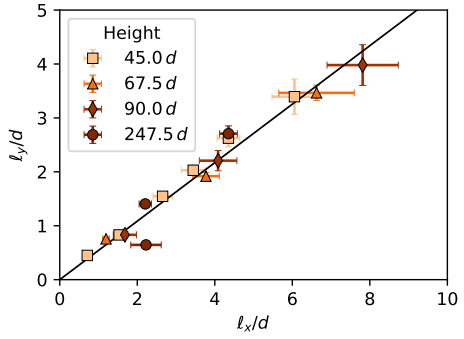

Fig. 4 Characteristic length of the fluctuations in the longitudinal direction, ℓ_y, as a function of the transverse one, ℓ_x. Each marker corresponds to a different column's initial height. Black line: linear fit of the data.

5 Conclusion

In this article, we performed a series of simulations of cohesive granular collapses and analyze the shape of their final deposit. As cohesion increases, the deposit features a stronger roughness, that we characterized. Quantitatively, we showed that the typical height of these fluctuations, based on the standard deviation of the roughness distribution, and the typical correlation length both increase linearly with the Bond number, namely with the material cohesion. These two lengths are correlated, resulting in a unique underlying length scale L, which corresponds to the cluster or aggregation size.

These results provide an easy visualization of the typical cohesive cluster size in the material, and yields a direct measurement of the inter-particle cohesion forces, while not requiring any heavy experimental setup. Moreover, the slight variation of these lengths with the collapse dynamics makes this measurement a fairly robust one. By increasing significantly the column's height, we highlighted a limit above which inertia plays a role in the roughness of the material, but we leave the influence of the dynamics on the roughness for further investigations.

Finally, from a fundamental point of view, how these fluctuations at the surface are related to the clusters in the bulk of the material remains unexplored. This could be investigated by measuring the porosity or density fluctuations, and could then explain how the presence of clusters translates into a different formulation for the rheology of the material. Indeed, a simple continuous rheology with a yield stress does not reproduce these roughness of at the surface of the deposit [13], meaning that a mere yield stress is not a sufficient ingredient. Recently, a lot of work was devoted to provide a cohesive rheology, based on numerical studies [37,38]. These rheologies show strong nonlocal effects and account for the observation of shear banding. Implementing such a rheology for free-surface flows could explain the properties of this cohesion-induced roughness.

Conflicts of interest

There are no conflicts to declare.

Acknowledgements

The authors warmly thank Adrien Gans for the experimental data, as well as Maxime Nicolas and Olivier Pouliquen for fruitful discussions. This work is part of the COPRINT project supported by the ANR grant ANR-17-CE08- 0017.

Notes and references

1 B. J. Ennis, *Powder technology*, 1996, **88**, 203–225.

2 M. V. Antequera, A. M. Ruiz, M. M. Perales, N. M. Munoz and M. J.-C. Ballesteros, *International journal of pharmaceutics*, 1994, **103**, 155–161.

3 T. T. Vo, S. Nezamabadi, P. Mutabaruka, J.-Y. Delenne, E. Izard, R. Pellenq and F. Radjai, *The European Physical Journal E*, 2019, **42**, 1–12.

4 P. S. Raux and A.-L. Biance, *Physical Review Fluids*, 2018, **3**, 014301.

5 S. Deboeuf and A. Fall, *Unsaturated wet granular flows over a rough incline: frictional and cohesive rheology*, arXiv2106.12258, 2021.

6 M. Scheel, R. Seemann, M. Brinkmann, M. Di Michiel, A. Sheppard, B. Breidenbach and S. Herminghaus, *Nature materials*, 2008, **7**, 189–193.

7 F. Tapia, S. Santucci and J.-C. Géminard, *EPL (Europhysics Letters)*, 2016, **115**, 64001.

8 A. Gans, O. Pouliquen and M. Nicolas, *Physical Review E*, 2020, **101**, 032904.

9 V. Richefeu, M. S. El Youssoufi and F. Radjai, *Physical Review E*, 2006, **73**, 051304.

10 P. Rognon, J.-N. Roux, D. Wolf, M. Naaïm and F. Chevoir, *EPL (Europhysics Letters)*, 2006, **74**, 644.

11 P. G. Rognon, J.-N. Roux, M. Naaim and F. Chevoir, *Journal of Fluid Mechanics*, 2008, **596**, 21–47.

12 D. Kadau, G. Bartels, L. Brendel and D. E. Wolf, *Computer Physics Communications*, 2002, **147**, 190–193.

13 A. Abramian, L. Staron and P.-Y. Lagrée, *Journal of Rheology*, 2020, **64**, 1227–1235.

14 S. Mandal, M. Nicolas and O. Pouliquen, *Proceedings of the National Academy of Sciences*, 2020, **117**, 8366–8373.

15 L. Staron, A. Abramian and P.-Y. Lagrée, EPJ Web of Conferences, 2021, p. 08006.

16 L. Staron and A. Abramian, 14th WCCM-ECCOMAS Congress 2020, 2021.

17 G. Lumay, F. Boschini, K. Traina, S. Bontempi, J.-C. Remy, R. Cloots and N. Vandewalle, *Powder technology*, 2012, **224**, 19–27.

18 J. J. Moreau, *European Journal of Mechanics-A/Solids*, 1994, **13**, 93–114.

19 L. Staron and E. Hinch, *Journal of Fluid Mechanics*, 2005, **545**, 1–27.

20 L. Staron and J. Phillips, *Physics of Fluids*, 2014, **26**, 033302.

21 S. T. Nase, W. L. Vargas, A. A. Abatan and J. McCarthy, *Powder Technology*, 2001, **116**, 214–223.

22 L. Ponson, *International Journal of Fracture*, 2016, **201**, 11–27.

23 B. B. Mandelbrot and J. W. Van Ness, *SIAM review*, 1968, **10**, 422–437.

24 D. Bonamy, L. Ponson, S. Prades, E. Bouchaud and C. Guillot, *Physical review letters*, 2006, **97**, 135504.

25 S. Santucci, K. J. Måløy, A. Delaplace, J. Mathiesen, A. Hansen, J. Ø. H. Bakke, J. Schmittbuhl, L. Vanel and P. Ray, *Physical review E*, 2007, **75**, 016104.

26 D. Bonamy and E. Bouchaud, *Physics Reports*, 2011, **498**, 1–44.

27 L. Ponson, H. Auradou, M. Pessel, V. Lazarus and J.-P. Hulin, *Physical Review E*, 2007, **76**, 036108.

28 H. Alarcon, J.-C. Géminard and F. Melo, *Physical Review E*, 2012, **86**, 061303.

29 E. Lajeunesse, A. Mangeney-Castelnau and J. Vilotte, *Physics of fluids*, 2004, **16**, 2371–2381.

30 E. Lajeunesse, J. Monnier and G. Homsy, *Physics of fluids*, 2005, **17**, 103302.

31 N. J. Balmforth and R. R. Kerswell, *Journal of Fluid Mechanics*, 2005, **538**, 399–428.
32 R. Artoni, A. C. Santomaso, F. Gabrieli, D. Tono and S. Cola, *Physical Review E*, 2013, **87**, 032205.
33 V. J. Langlois, A. Quiquerez and P. Allemand, *Journal of Geophysical Research: Earth Surface*, 2015, **120**, 1866–1880.
34 A. C. Santomaso, S. Volpato and F. Gabrieli, *Physics of Fluids*, 2018, **30**, 063301.
35 A. Bougouin, L. Lacaze and T. Bonometti, *Physical Review Fluids*, 2019, **4**, 124306.
36 A. Gans, *PhD thesis*, Aix-Marseille Université, 2021.
37 S. Mandal, M. Nicolas and O. Pouliquen, *Physical Review X*, 2021, **11**, 021017.
38 M. Macaulay and P. Rognon, *Soft matter*, 2021, **17**, 165–173.